J. Fluid Mech. (1967), *vol.* 30, *part* 2, *pp.* 209–224
Printed in Great Britain

Stability of the developing laminar flow in a parallel-plate channel

By T. S. CHEN† AND E. M. SPARROW
University of Minnesota, Minneapolis, Minnesota

(Received 20 January 1967 and in revised form 20 June 1967)

The hydrodynamic stability of the developing laminar flow in the entrance region of a parallel-plate channel is investigated using the theory of small disturbances. The stability of the fully developed flow is also re-examined. A wide range of analytical (i.e. asymptotic) and numerical methods are employed in the stability investigation. Among the asymptotic methods, each of three viscous solutions (singular, regular and composite) is used along with the inviscid solution to provide critical Reynolds numbers and complete neutral stability curves. Two numerical methods, finite differences and stepwise integration, are applied to calculate critical Reynolds numbers. The basic flow in the development region is treated from two stand-points: as a channel velocity profile and as a boundary-layer velocity profile. Extensive comparisons among the various methods and flow models disclose their various strengths and ranges of applicability. As a general result, it is found that the critical Reynolds number decreases monotonically with increasing distance from the channel entrance, approaching the fully developed value as a limit.

1. Introduction

It is well established from the theory of small disturbances that the fully developed flow in a parallel-plate channel (i.e. the plane Poiseuille flow) is unstable for large Reynolds numbers. The stability characteristics of the hydrodynamically developing flow in the entrance region of a parallel-plate channel have, however, been investigated only in a preliminary and incomplete manner. The only study available up to this time is that of Hahneman, Freeman & Finston (1948). In lieu of a detailed mathematical treatment of the problem, these authors confined themselves to the computation of critical Reynolds numbers by applying the approximate formulae deduced by Lin (1945) from the zeroth-order asymptotic solution of the disturbance equations. As is demonstrated later, these formulae do not provide accurate results in the development region because conditions postulated in their derivation are not fulfilled. Moreover, the basic flow profiles (Schlichting 1934) used in the calculations do not give velocity derivatives with good accuracy. As is well known, such derivatives play

† Present address: Department of Mechanical Engineering, University of Missouri at Rolla, Rolla, Missouri.

an important role in the final results of the stability calculations. This probably accounts for the large scatter among the calculated points in the plot of critical Reynolds number versus axial location shown by Hahneman *et al.*

The present research constitutes a detailed investigation of the stability of the entrance region flow and has two objectives: first, to provide detailed and reliable stability information such as neutral stability curves and critical Reynolds numbers; and secondly, to make certain contributions to the mathematical and computational procedures involved in asymptotic stability theory. To achieve these ends, a wide variety of analytical and numerical methods of solution have been employed. The flow in the hydrodynamic entrance region appears to be, in some respects, a boundary-layer flow. Correspondingly, the stability characteristics of a boundary-layer model of the developing flow are evaluated in addition to the stability characteristics of the complete velocity profiles of the developing flow.

Owing to the wide-ranging nature of the present study, it has been necessary to omit many details because of space limitations. These are available in Chen (1966).

2. Formulation of the problem

Before proceeding to the stability problem, consideration is given first to the basic flow in the hydrodynamic development region of the channel. Among the various approximate analytical solutions available in the literature, that of Sparrow, Lin & Lundgren (1964) appears to offer the most complete and accurate results. They obtained closed-form velocity solutions which are continuous over the cross-section and along the length all the way from the entrance to the fully developed region. This feature is of advantage in the execution of the stability problem, because the velocity derivatives are continuous and can be evaluated with great accuracy from algebraic expressions.

With the transverse co-ordinate measured from the bottom wall of the channel, the velocity solution given by Sparrow *et al.* reduces to the form

$$U = 1{\cdot}5(2y - y^2) + \sum_{i=1}^{\infty} \frac{2}{\alpha_i^2}\left[\frac{\cos\alpha_i(y-1)}{\cos\alpha_i} - 1\right]\exp\{-\alpha_i^2 X^*\} \tag{1}$$

in which α_i are the roots of $\tan\alpha_i = \alpha_i$, and

$$U = \bar{u}/\bar{u}_{\mathrm{av}}, \quad y = \bar{y}/L, \quad X^* = \bar{x}^*/LR^*, \tag{2}$$

where $\bar{u}$ and $\bar{u}_{\mathrm{av}}$ are, respectively, the local velocity of the basic flow and its average value; L is the half-width of the channel; $R^* = L\bar{u}_{\mathrm{av}}/\nu$ is the Reynolds number, ν being the kinematic viscosity; $\bar{y}$ is the physical co-ordinate normal to the flow direction; and $\bar{x}^*$ is a stretched axial co-ordinate. The relationship between X^* and the physical axial co-ordinate X is available in graphical form from Sparrow and in tabular form from Chen.

If the basic flow $\bar{u}$ is assumed to be parallel, i.e., $\bar{u} = \bar{u}(\bar{y})$, upon which are superposed two-dimensional small disturbances, and if it is further postulated that both the basic flow and the resultant flow satisfy the Navier–Stokes equa-

tions of motion, there is obtained the familiar Orr–Sommerfeld equation in dimensionless form

$$(W-c)(\phi''-\alpha^2\phi)-W''\phi = -\frac{i}{\alpha R}(\phi^{iv}-2\alpha^2\phi''+\alpha^4\phi). \tag{3}$$

In this equation, W and $c(=c_r+ic_i)$ represent, respectively, the basic flow velocity and the wave velocity normalized by a characteristic velocity, say, $\overline{u}_{max}$, the maximum velocity at centre of the channel; α is the wave-number based on a characteristic length, say, L; $R = L\overline{u}_{max}/\nu$ is the Reynolds number based on $\overline{u}_{max}$; and the primes denote differentiation with respect to y. It may be noted that the treatment of (1) as a family of parallel flows with X^* as a parameter is consistent with the basic assumption $\alpha R \gg 1$.

The amplitude function ϕ is related to the stream function ψ by the expression

$$\psi(x,y,t) = \phi(y)\exp\{i\alpha(x-ct)\}. \tag{4}$$

If c_i is negative, the disturbances decay and the flow is stable; while if it is positive, the disturbances are amplified and the flow is unstable. The condition of neutral stability is characterized by $c_i = 0$.

Equation (3) is a homogeneous, linear differential equation of the fourth order. There exists, therefore, a set of four linearly independent solutions which are analytic functions of y and of the parameters c, α and R. This set of solutions will be denoted by $\phi_1(y)$, $\phi_2(y)$, $\phi_3(y)$ and $\phi_4(y)$.

The boundary conditions for ϕ are different depending upon whether the stability problem is formulated in terms of a channel flow or a boundary-layer flow. Owing to the symmetry of the basic flow profile with respect to the centre line of the channel, the solution $\phi(y)$ for channel flow may be divided into even and odd modes. Of primary interest, however, is the case of even $\phi(y)$, because the work of Gröhne (1954) strongly suggests that, for plane Poiseuille flow, only this mode is likely to lead to instabilty. If $\phi(y)$ is an even function, the boundary conditions are

$$\phi(y_1) = \phi'(y_1) = \phi'(y_2) = \phi'''(y_2) = 0 \tag{5}$$

where, for notational convenience, y_1 and y_2 represent, respectively, the values of y at the bottom wall (i.e. $y_1 = 0$) and at the centre of the channel (i.e. $y_2 = 1$).

When the basic flow is regarded as a boundary-layer flow, the condition to be satisfied at the edge of the boundary layer $\overline{y}_2 = \overline{\delta}$ (defined here as the distance from the wall where $\overline{u} = \overline{u}_\delta = 0{\cdot}999\overline{u}_{max}$) is readily shown to be

$$\phi' + \alpha\phi = 0 \quad \text{for} \quad y \geqslant y_2 = \delta \tag{6}$$

and $\phi(y_1) = \phi'(y_1) = 0$ as before.

3. The asymptotic solutions

The asymptotic solutions of (3) are given elsewhere (see, for example, Heisenberg 1924; Lin 1945, 1955; Tollmien 1929, 1947; Stuart 1963; Shen 1964; and Reid 1965). It suffices here to give only the final expressions.

For the inviscid flow, the right-hand side of (3) vanishes. The resulting equation is of the second order and yields two solutions ϕ_1 and ϕ_2 which, following Heisenberg (1924), are

$$\phi_1 = (W-c)\sum_{n=0}^{\infty}\alpha^{2n}h_{2n}(y), \quad \phi_2 = (W-c)\sum_{n=0}^{\infty}\alpha^{2n}k_{2n+1}(y) \tag{7}$$

in which $h_0 = 1$ and all other h and k are expressed as integrals (see, for instance, Lin 1945). The solutions ϕ_1 and ϕ_2 are singular at $y = y_c$ where $W = c$.

There are three sets of viscous solutions which are of interest in connexion with the present investigation. The other asymptotic method of Heisenberg gives the singular viscous solutions (cf. Heisenberg 1924; Lin 1945)

$$\phi_j = (W-c)^{-\frac{5}{4}}\exp\left\{\pm\int_{y_c}^{y}[i\alpha R(W-c)]^{\frac{1}{2}}dy\right\} \quad (j = 3, 4), \tag{8}$$

in which the minus sign corresponds to $j = 3$ and the plus sign to $j = 4$. It is to be noted that ϕ_3 and ϕ_4 are singular at the turning point y_c where $W = c$ and are valid for $(y-y_c) \neq 0$ fixed and $(\alpha R)\to\infty$.

For asymptotic solutions which are valid in the region $(y-y_c)\to 0$ as $(\alpha R)\to\infty$, one may refer, for example, to the work of Lin (1945) and of Shen (1964). The outcome of the zeroth-order approximation gives two regular viscous solutions

$$\chi_j = \int_{\pm\infty}^{\zeta}d\gamma\int_{\pm\infty}^{\gamma}v^{\frac{1}{2}}H_{\frac{1}{3}}^{(j-2)}[\tfrac{2}{3}(iv)^{\frac{3}{2}}]dv, \quad (j = 3, 4). \tag{9}$$

The $\pm$ signs correspond respectively to $j = 3$ and $j = 4$, and

$$\zeta = (\alpha R W_c')^{\frac{1}{3}}(y-y_c). \tag{9a}$$

The solutions χ_3 and χ_4 are valid for ζ fixed and $(\alpha R)\to\infty$ (i.e. $y\to y_c$) and are regular at y_c.

The fact that ϕ_3 and ϕ_4 are not uniformly valid at $y = y_c$ and χ_3 and χ_4 become increasingly inaccurate as $|y-y_c|$ becomes large motivates a combining of these solutions such that the resulting solutions will be uniformly valid in both relevant limits. This matching was first performed by Tollmien (1947) for the neutral case. The final expressions for the composite solutions take the form (see also Lin 1955; Reid 1965)

$$\hat{\chi}_j = \left(\frac{\hat{\zeta}}{W-c}\right)^{\frac{5}{4}}\int_{\pm\infty}^{\hat{\zeta}}d\gamma\int_{\pm\infty}^{\gamma}v^{\frac{1}{2}}H_{\frac{1}{3}}^{(j-2)}[\tfrac{2}{3}(iv)^{\frac{3}{2}}]dv, \quad (j = 3, 4), \tag{10}$$

where the $\pm$ signs have the same meaning as in (9), and

$$\hat{\zeta} = \left[\frac{3}{2}\int_{y_c}^{y}[\alpha R(W-c)]^{\frac{1}{2}}dy\right]^{\frac{2}{3}}. \tag{10a}$$

4. The eigenvalue problems

Having delineated the different sets of asymptotic solutions, one can now proceed to formulate the eigenvalue problems for subsequent numerical evaluation. For this purpose, one may alternatively use: (i) the four asymptotic solutions

ϕ_1, ϕ_2, ϕ_3 and ϕ_4; (ii) the combination ϕ_1, ϕ_2, χ_3 and χ_4; or (iii) the four solutions ϕ_1, ϕ_2, $\hat{\chi}_3$ and $\hat{\chi}_4$.

The formulation of the eigenvalue problems follows closely the approach of Lin (1945), except that different and more efficient methods were employed here in the evaluation of the viscous solutions and the series coefficients in the inviscid solutions. A secular equation embodying the homogeneous boundary conditions is formed and then simplified on the basis of order of magnitude arguments. From these operations, there follows

$$1+W_1'c\frac{\phi_{22}'}{\phi_{12}'}=\left[1+\frac{W_1'}{c}\frac{\phi_{31}}{\phi_{31}'}\right]^{-1}, \quad 1+W_1'c\frac{\phi_{22}'+\alpha\phi_{22}}{\phi_{12}'+\alpha\phi_{12}}=\left[1+\frac{W_1'}{c}\frac{\phi_{31}}{\phi_{31}'}\right]^{-1} \tag{11}$$

respectively for channel flow and for boundary-layer flow. In the foregoing, $W_1'=W'(y_1)$ and ϕ_{12}, ϕ_{31}, ϕ_{22}', etc. stand for $\phi_1(y_2)$, $\phi_3(y_1)$, $\phi_2'(y_2)$, etc.

It is of interest to note that the right-hand sides (i.e. the viscous terms) of (11) are identical. Thus, if one defines the inviscid function on the left-hand side of each of the equations as $(u+iv)$, identical eigenvalue equations can be derived for subsequent numerical evaluation of the neutral stability curves. The only difference, in addition to the different definitions of $(u+iv)$, is that in the boundary-layer model the boundary-layer thickness $\bar{\delta}$ and the velocity at $\bar{\delta}$, $\bar{u}_\delta$, are used, respectively, to normalize all the lengths and velocities.

The quantities $(u+iv)$ for channel flow and boundary-layer flow are respectively defined as

$$u+iv=1+W_1'c\frac{\phi_{22}'}{\phi_{12}'}; \quad u+iv=1+W_1'c\frac{\phi_{22}'+\alpha\phi_{22}}{\phi_{12}'+\alpha\phi_{12}}. \tag{12}$$

In view of (7), it is evident that both forms for $(u+iv)$ can be written in terms of power series in α^2. These series representations may be found in Lin (1945).

Having dealt with the representations for $(u+iv)$, one can now proceed to specialize the right-hand sides of (11) for the different viscous solutions. For the singular viscous solution, the expression for ϕ_3, equation (8), leads to (cf. Lin 1955)

$$u+iv=1+[Z^{\frac{3}{2}}e^{-\frac{1}{4}\pi i}-\tfrac{9}{4}]^{-1}, \tag{13}$$

where

$$Z=c(\alpha R/W_1'^2)^{\frac{1}{3}}. \tag{13a}$$

Alternatively, if (9) for χ_3 is used to evaluate the quantity ϕ_{31}/ϕ_{31}', the regular viscous solution yields

$$u+iv=[1-(1+\lambda)F(z)]^{-1}. \tag{14}$$

Similarly, the composite viscous solution $\hat{\chi}_3$, equation (10), gives

$$u+iv=[1-(1+\hat{\lambda})\hat{F}(\hat{z},c)]^{-1}. \tag{15}$$

The qualities z and $\hat{z}$ appearing in the foregoing are respectively equal to $-\zeta$ and $-\hat{\zeta}$, in which $y=y_1$. In addition, λ and $\hat{\lambda}$ are defined by

$$W_1'(y_c-y_1)=c(1+\lambda); \quad W_1'\left[\frac{3}{2\sqrt{c}}\int_{y_1}^{y_c}(c-W)^{\frac{1}{2}}dy\right]=c(1+\hat{\lambda}) \tag{16}$$

the bracketed factor being termed $(\hat{y}_c-\hat{y}_1)$.

The function $F(z)$ (or $F(\hat{z})$) is the well-known Tietjens function, while $\hat{F}(\hat{z}, c)$ is related to $F(\hat{z})$ as follows

$$\hat{F}(\hat{z}, c) = F(\hat{z})/\{1+\tfrac{5}{4}[1-(W_1'/c)(\hat{y}_c-\hat{y}_1)]F(\hat{z})\}. \tag{17}$$

$F(z)$ was first computed by Tietjens (1925) and has subsequently been evaluated to greater accuracy (see, for instance, Lin 1945; Holstein 1950; Lock 1954; Miles 1960). Very recently, Chen, Joseph & Sparrow (1966) have reduced $F(z)$ to a ratio of rapidly convergent power series. This series representation can be incorporated directly into a computer program, thereby facilitating a completely computerized procedure for calculating eigenvalues from asymptotic solutions.

Equations (13), (14) and (15) are, respectively, the final eigenvalue equations for the singular viscous, the regular viscous† and the composite† solutions. These formulae are valid for both the channel flow and the boundary-layer models, with the corresponding $(u+iv)$ respectively expressed by the first and second members of (12).

For each one of the just-outlined eigenvalue problems, the method of successive iterations has been employed to generate neutral stability curves. For instance, for the regular viscous solution, iterative solution of (12) and (14) yields α and z for a given real c. Then, the converged values of α and z are used to calculate the Reynolds number from the relation $z = (\alpha R W_c')^{\frac{1}{3}}(y_c-y_1)$, W_c' and (y_c-y_1) having been determined beforehand. A similar approach was employed for the singular viscous and composite solutions. The computational details may be found in Chen (1966).

5. Lin's formulae for estimation of critical Reynolds and wave-numbers

Approximate formulae for the estimation of the critical Reynolds number and the corresponding wave-number have been derived by Lin (1945) by simplifying the regular viscous solution, assuming that the critical Reynolds number occurs at $z = 3{\cdot}21$ and that α and c are small. The end results are: for a symmetric profile with ϕ even

$$\alpha = [W_1'c/H_1(0)]^{\frac{1}{2}}, \quad R = \frac{30W_1'}{c^3}[W_1'H_1(0)/c]^{\frac{1}{2}}, \quad H_1(0) = \int_{y_1}^{y_2} W^2 dy; \tag{18}$$

for a boundary-layer profile

$$\alpha_\delta = W_1'c, \quad R_\delta = 25W_1'/c^4, \tag{19}$$

where $\alpha_\delta = \bar{\alpha}\bar{\delta}$ and $R_\delta = \bar{u}_\delta\bar{\delta}/\nu$. In the foregoing, $c = W_c$ is found from the expression

$$0{\cdot}58 = -\pi W_1'c\frac{W_c''}{W_c'^3}\left[3+2\frac{W_1'}{c}(y_1-y_c)\right]. \tag{20}$$

Equations (18) and (20) were employed by Hahneman *et al.* (1948) in their study of the stability of the entrance region flow in a parallel-plate channel. As will be demonstrated in the forthcoming presentation of results, these formulae give good estimates for the critical Reynolds number only for profiles which are nearly fully developed, and fail to give accurate critical Reynolds numbers near the entrance of the channel.

† For the purpose of calculation, F and $\hat{F}$ were respectively replaced by the modified Tietjens functions $\mathscr{F}$ and $\hat{\mathscr{F}}$.

6. Stepwise integration and finite-difference methods of solution

Two numerical schemes were employed to solve the Orr–Sommerfeld equation. These techniques have been treated in detail by previous workers and need not be repeated here. They were used in this investigation to test and confirm their utility *vis-à-vis* the asymptotic method of solution. An interesting difference between the eigenvalue problem encountered in the numerical solutions and that of the asymptotic solutions is that in the former c is found for given α and R, while in the latter, α and R are found for given c.

In the stepwise integration scheme, the method due to Nachtsheim (1964) was adopted, with minor modifications in the computer program. The Nachtsheim formulation, in essence, treats the boundary value problem as an initial value problem. This is done by a step-by-step numerical integration of the disturbance equation, with assigned values of α and R and an assumed value of c; c is varied iteratively. In carrying out the actual integrations, it is necessary to assign provisionally certain initial values, and it is the essence of the problem to find the correct initial values so that the differential equation and boundary conditions are identically satisfied. To minimize the effects of the truncation error, the solution is carried out in two parts: by starting at the wall ($y = y_1 = 0$) and integrating forward, by starting at the centre of the channel ($y = y_2 = 1$) and integrating backward, and then matching somewhere in between, say, at $y = 0{\cdot}5$. This process is continued until the matching condition is satisfied. Unfortunately, the stepwise integration method proved to be successful only for the fully developed flow and for the developing flow adjacent to the developed region.

The finite-difference scheme is due to Thomas (1953). His technique involves transformation of the Orr–Sommerfeld equation and its boundary conditions into a set of algebraic equations, with special care taken to reduce the truncation error. The details of the transformation and the formulation of the simultaneous algebraic equations have been presented by Thomas (1953), Kurtz & Crandall (1962), and Tsou (1965). In the present investigation, a simplified and more efficient computer program (relative to that of prior investigators) was devised to determine the eigenvalues. It was also found that the effect of the mesh size on the accuracy of the eigenvalues is significant, especially as the duct inlet is approached, the mesh size having to be decreased to maintain the accuracy of the results.

7. The neutral stability results

The asymptotic solutions yielded complete neutral stability curves as well as critical Reynolds and wave-numbers. On the other hand, the finite-difference and stepwise integration schemes provided only critical Reynolds and wave-numbers. A detailed tabulation of the computed results can be found in the thesis (Chen 1966) from which this paper is drawn. Only the graphical results will be presented here.

Fully developed flow. Figure 1 is a plot of neutral stability results for the case of fully developed flow, each of the three curves corresponding to a different

viscous solution. In the abscissa of the plot, $R(=\bar{u}_{\max}L/\nu)$ is used. If a vertical line is drawn tangent to the nose of each curve, the critical Reynolds number $R_{\rm cr}$ is obtained. This gives $R_{\rm cr}$ = 5400, 420 and 980 for the regular viscous, the composite, and the singular viscous solutions, respectively.† The composite solution yields a neutral curve which has a shape similar to that obtained for the regular viscous solution. Both the lower and the upper branches of these curves

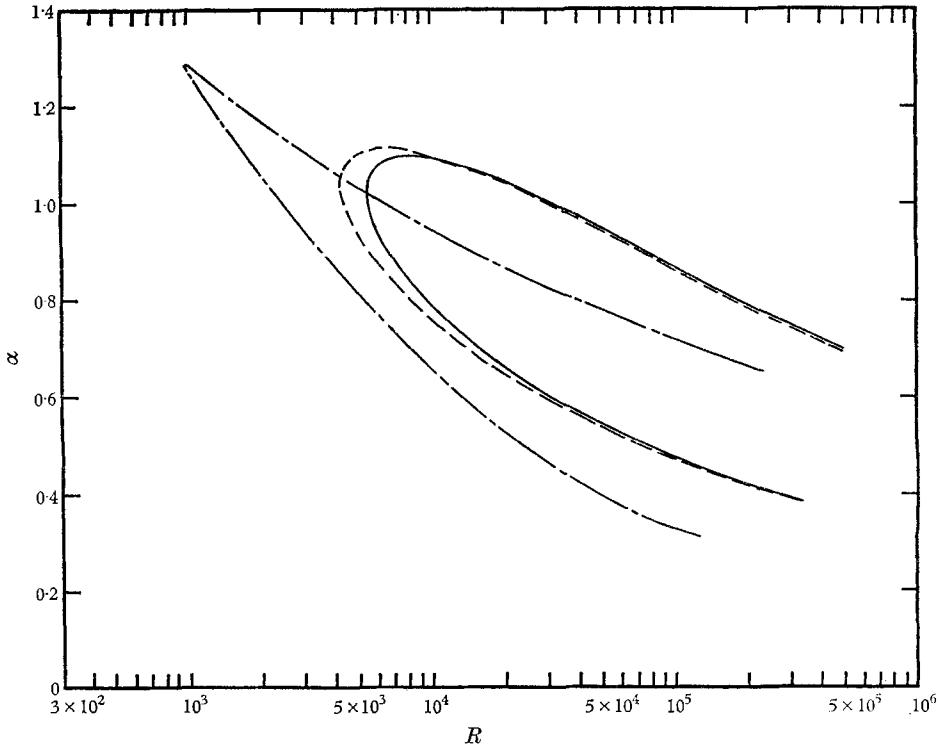

FIGURE 1. Neutral stability curves for the fully developed flow, various viscous solutions. ——, regular viscous solution; – – –, composite solution; — — —, singular viscous solution.

are almost coincident. There is, however, a deviation near the noses of the curves amounting to a difference of about 20 % in the critical Reynolds number. The singular viscous solution gives rise to a neutral curve which is quite different from the other two; this is the curve that would have been obtained by Heisenberg (1924) had he completed the neutral stability computation.

The singular viscous solutions ϕ_3 and ϕ_4 give an error which is usually assigned the order $(\alpha R)^{-\frac{1}{2}}$, while the error in the regular viscous solutions χ_3 and χ_4 is regarded as being on the order of $(\alpha R)^{-\frac{1}{3}}$ (see, for example, Lin 1945). Thus, at first glance, it might appear that for large (αR), the ϕ solutions are computationally superior to the χ solutions. However, this is not the case. The error estimate

† These results will subsequently be compared with the $R_{\rm cr}$ from the finite difference solutions.

for the ϕ solutions is not uniform; in fact, these solutions are singular at $y = y_c$ and are not accurate near y_c where $|y - y_c|$ is of the order of $(\alpha R)^{-\frac{1}{3}}$. For the type of basic flow studied here, y_c is sufficiently small so that the region $|y - y_c| \sim (\alpha R)^{-\frac{1}{3}}$ occupies essentially the entire layer between y_c and the wall. Correspondingly, the ϕ solutions are of low accuracy in the aforementioned layer; on the other hand, the χ solutions are of high accuracy there. The superior performance of the χ solutions therefore becomes plausible. On the other hand, the somewhat inferior performance of the composite solution, relative to the regular viscous solution, is a bit surprising. This interesting finding requires further examination.†

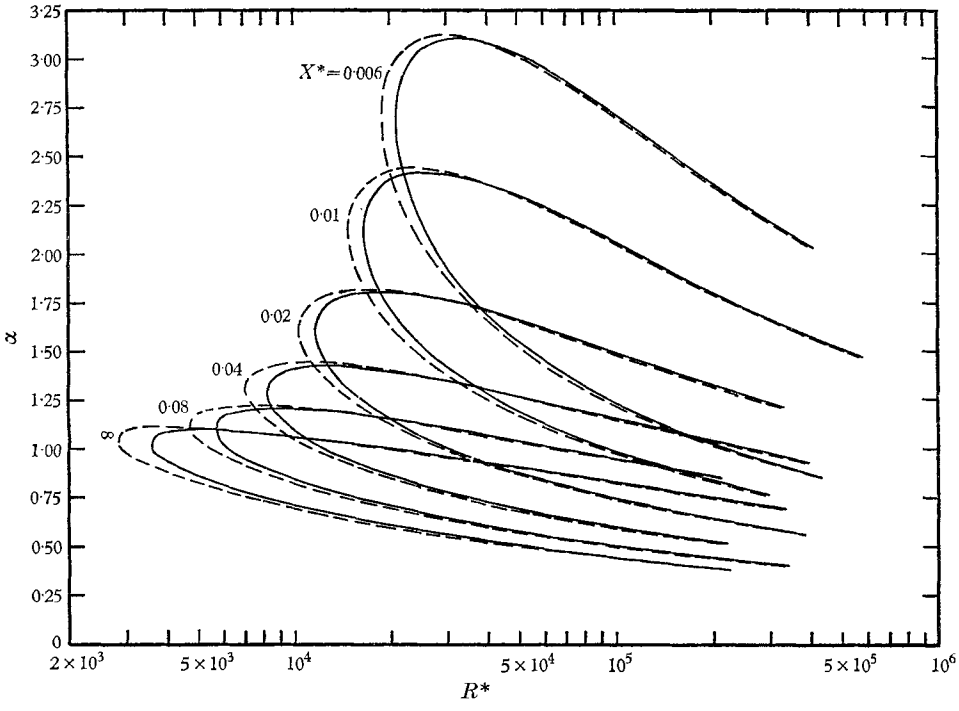

FIGURE 2. Neutral stability curves for several axial locations, channel profile, regular viscous and composite solutions. ——, regular viscous solutions; – – –, composite solution.

Developing flow. Neutral stability results based on the channel flow model were obtained for the regular viscous and the composite solutions at 13 axial locations X^* ranging from 0·005 to 0·20. In order to preserve clarity, neutral curves are shown in figure 2 for only five axial locations. Included also are the

† The composite solution employed here can be reduced to ϕ and χ solutions in both relevant limits $|\hat{\zeta}|$ large and $|y - y_c|$ small and is valid for any values of c, small or large. An alternative approach has been presented by Reid (1965) wherein the slowly varying term $[\hat{\zeta}/(W-c)]^{\frac{5}{4}}$ is treated as a constant. In this instance, $\hat{F}(\hat{z}, c)$ reduces to $F(\hat{z})$. The results of his calculations for plane Poiseuille flow are in closer agreement with those of the finite-difference scheme than the present ones using $\hat{F}(\hat{z}, c)$. However, his formula can be reduced only to the χ solutions and not to the ϕ solutions. These two different approaches are discussed in detail by Fu (1967).

two curves from the fully developed flow, that is, $X^* = \infty$. In the plot, R^* $(= \bar{u}_{av} L/\nu)$ is used in the abscissa instead of $R(= \bar{u}_{max} L/\nu)$. This choice was made because R^* contains no x-dependent quantities, whereas R contains $\bar{u}_{max}$, which depends on X^*.

A study of figure 2 reveals that both the critical Reynolds number and the critical wave-number increase as X^* decreases. That is, the flow becomes more and more stable as one approaches closer and closer to the entrance of the channel. Again, the composite solution yields somewhat lower critical Reynolds numbers than the regular viscous solution; the differences range from 22 to 9 % as X^* ranges from 0·20 to 0·005.

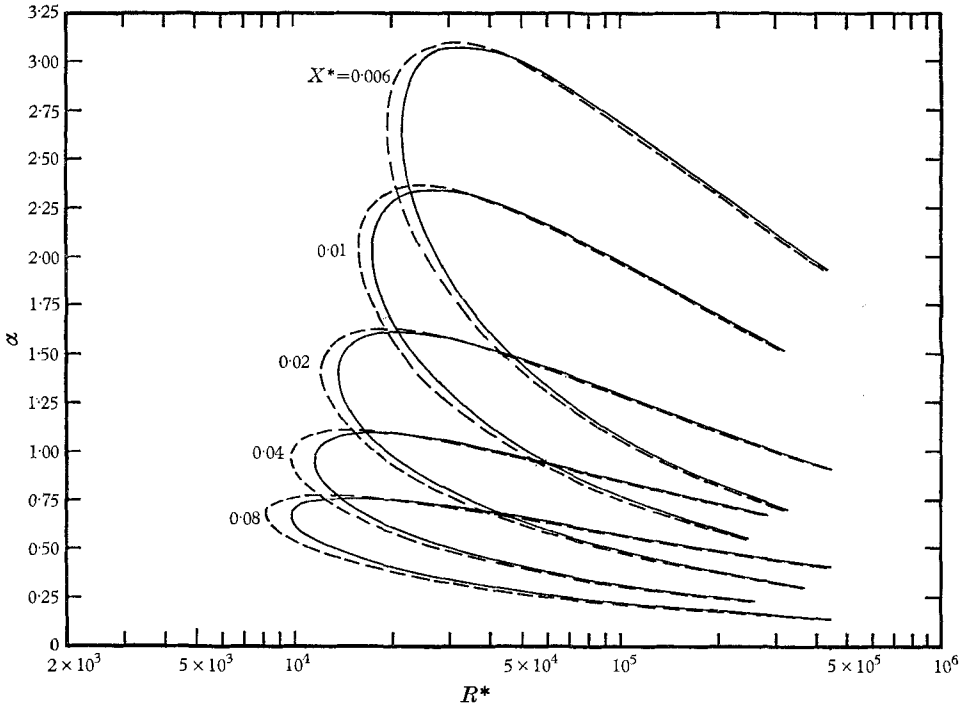

FIGURE 3. Neutral stability curves for several axial locations, boundary-layer profile, regular viscous and composite solutions. ——, regular viscous solution; – – –, composite solution.

For the boundary-layer model of the basic flow, the neutral stability results were computed for 11 axial locations X^* ranging from 0·005 to 0·10. As in the case of the channel profile, only the regular viscous and the composite solutions were carried out. The neutral curves for five axial locations are illustrated in figure 3. In this plot, α and R^* are again used as co-ordinates. These curves show, as for the channel profile, that the critical Reynolds number and the critical wave-number increase as X^* decreases. As before, the composite solution gives somewhat lower critical Reynolds numbers.

In order to show the relationship between the channel and the boundary-layer models, neutral curves for five axial locations in the upstream portion of the

entrance region are brought together in figure 4; all results are from the regular viscous solution. It is of interest to note from the figure that for small X^* (i.e. for axial locations near the entrance of the channel), the two models predict practically identical neutral stability results. As X^* increases, the discrepancy becomes more and more pronounced. This is due to the fact that the boundary-layer model loses validity for large values of X^*.

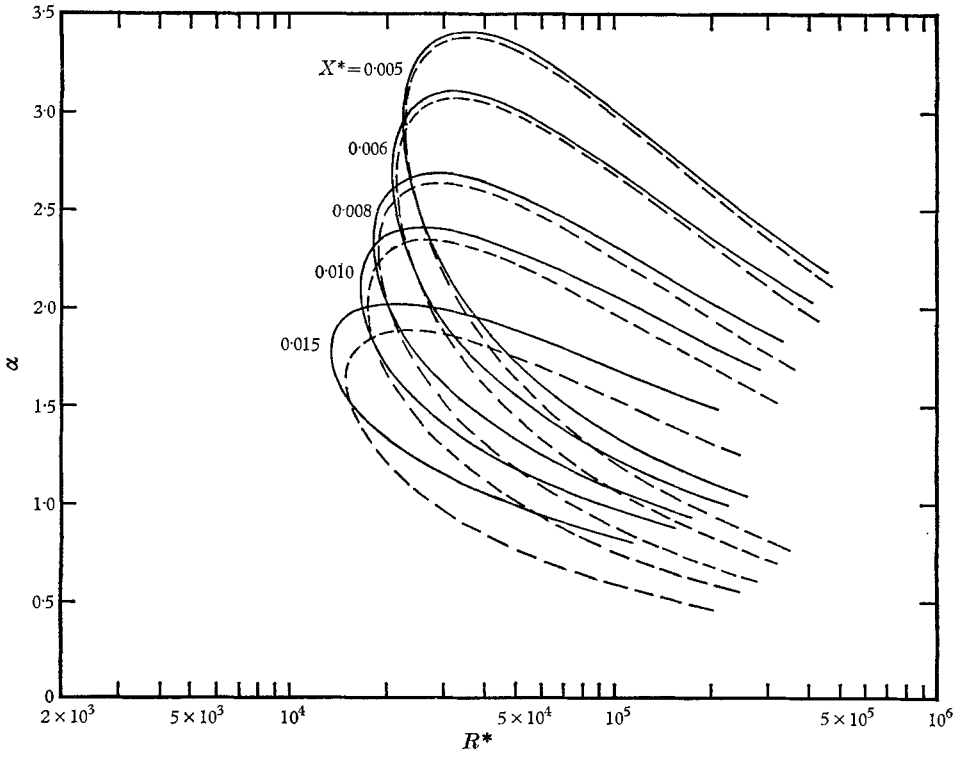

FIGURE 4. Comparison of neutral stability curves from channel and boundary-layer profiles, regular viscous solution. ——, channel flow; – – –, boundary-layer flow.

8. The stability boundaries

The critical Reynolds numbers R^*_{cr} for the channel profiles are plotted as a function of X^* in figure 5. This presentation includes results from the various sets of asymptotic solutions and from the stepwise integration and the finite-difference schemes. The results from the stepwise integration scheme for $X^* \geqslant 0{\cdot}06$† are essentially identical to those from the finite-difference scheme. The two curves, therefore, lie together as illustrated in the figure. The general characteristic of all the R^*_{cr} versus X^* curves is that the critical Reynolds number decreases monotonically, as X^* increases, to a constant value for the fully developed flow.

If it is assumed that the results from the finite-difference scheme are numerically

† The stepwise integration method did not function successfully with single-precision computer arithmetic for X^* smaller than 0·06.

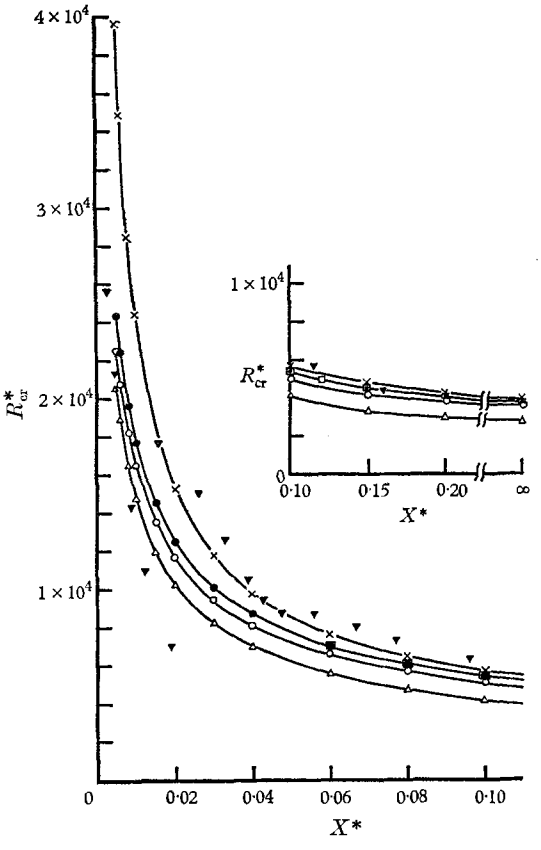

FIGURE 5. Critical Reynolds number versus axial location, channel profile, analytical and numerical methods of solution. —□—, stepwise integration scheme; —●—, finite-difference scheme; —○—, regular viscous solution; —△—, composite solution; —×—, Lin's formulae, equations (18) and (20); ▼, Hahneman, Freeman & Finston (1948).

exact, then it is logical to take them as a standard of comparison for the other results. It is evident from the figure that the regular viscous solution yields a curve which closely follows that from the finite-difference scheme, showing critical Reynolds numbers somewhat on the low side. The composite solution results in still lower critical Reynolds numbers.

It may be of interest to compare the various critical Reynolds numbers obtained for the fully developed flow. The regular viscous solution yielded a value $R_{cr} = 5400$, while the finite-difference method gave $R_{cr} = 5775$ (mesh size of 0·01). From the step-wise integration scheme, values of 5758 and 5769 were obtained using mesh sizes of 0·01 and 0·005. For purposes of comparison, it may be noted that values of 5300 and 5780 have been calculated by Lin (1945) and by Thomas (1953), respectively, from the regular viscous solution and the finite-difference method.

Lin's approximate formulae, (18) and (20), give surprisingly good agreement with the finite-difference scheme for large values of X^*; that is, for profiles which

are nearly fully developed.† The discrepancy increases markedly as X^* decreases toward the entrance of the channel and reaches 86 % (on the high side) at $X^* = 0{\cdot}005$. This large error in the predictions afforded by Lin's formulae at small X^* is attributed to the invalidity of α and c both being small, as assumed in the derivation. The phase velocity c_r is indeed small (about 0·31 at $X^* = 0{\cdot}005$), but the critical wave number α_{cr} increases to about 3·0 as X^* decreases to 0·005.

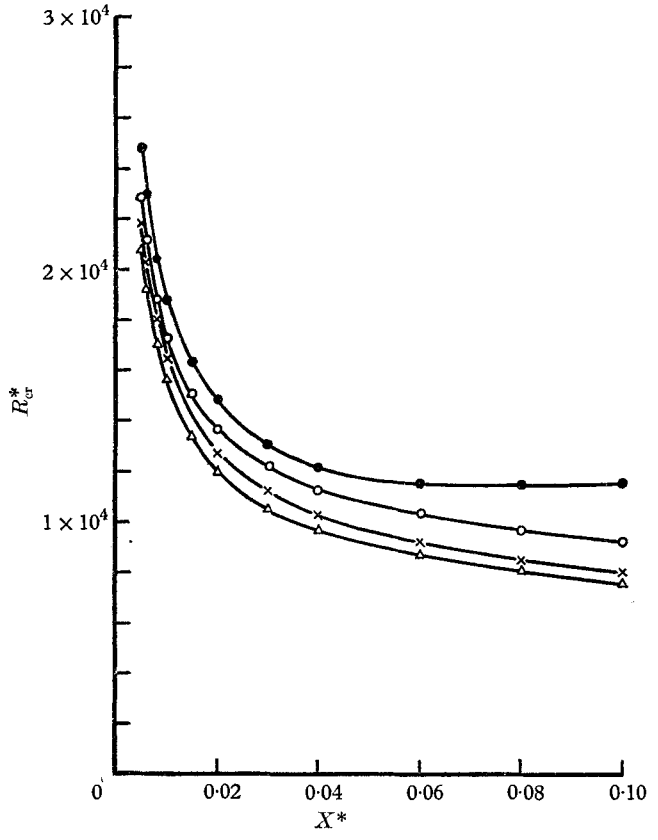

FIGURE 6. Critical Reynolds number versus axial location, boundary-layer profile, analytical and numerical methods of solution. —●—, finite-difference scheme; —○—, regular viscous solution; —△—, composite solution; — × —, Lin's formulae, equations (19) and (20).

Equations (18) and (20) were employed by Hahneman *et al.* (1948) in their study of the stability of developing flow in a parallel-plate channel. Their results were converted to R^*_{cr} as a function of X^* and are included in figure 5. It is to be noted that there is a wide scatter among the points for X^* smaller than 0·03. This is probably due to inaccuracies in the velocity profiles used in the calculations. The discussion in the preceding paragraph suggests that the solution method used by Hahneman is not able to provide accurate stability results in the entrance region.

The critical Reynolds numbers corresponding to the boundary-layer model are illustrated in figure 6. In this plot, the finite-difference scheme shows the highest

† For the fully developed flow, (18) and (20) yielded $R_{cr} = 5875$.

critical Reynolds numbers among the various solutions. For X^* larger than 0·04, it appears that the boundary-layer model, when solved by finite-differences, is invalid. Indeed, the curve starts to level off and then tends to rise at $X^* = 0{\cdot}10$. This behaviour is believed due to the effect of the value of W'' at the edge of the boundary layer. For larger values of X^*, the imposed condition that $W'' = 0$ at $y \geqslant \delta$ is not satisfied at all (as a limit, $W'' = -2$ for the fully developed flow).

The regular viscous and the composite solutions give critical Reynolds numbers which are lower than those obtained from the finite-difference scheme. In the determination of the critical Reynolds numbers by the asymptotic methods, W'' does not appear at all. Only W' at the wall and at the turning point y_c are involved in the calculations. It is, therefore, conjectured that the curves from the asymptotic solutions show the correct trend for the larger values of X^*.

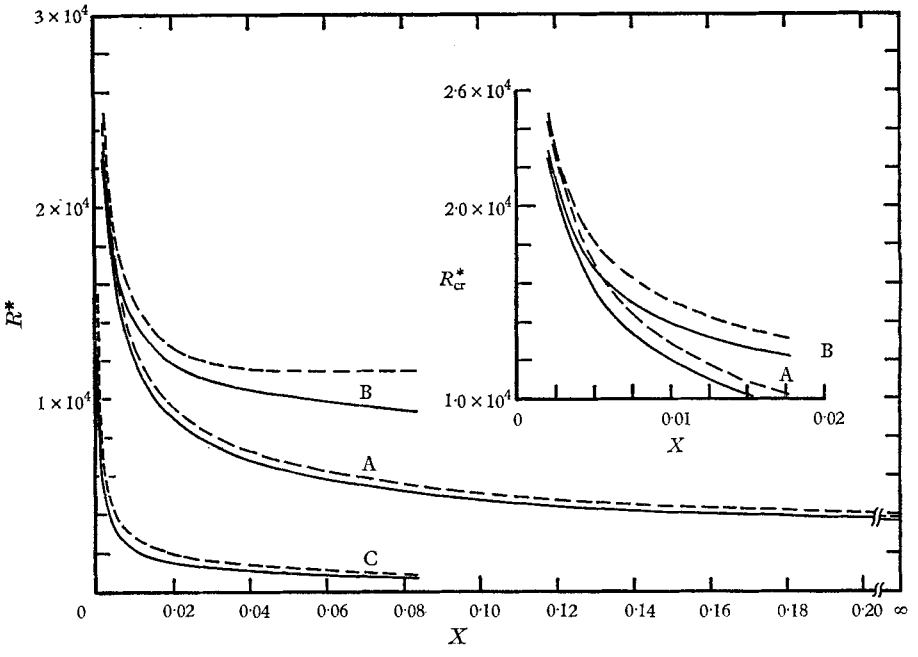

FIGURE 7. Critical Reynolds number versus (dimensionless) physical axial co-ordinate. channel and boundary-layer profiles. – – –, finite-difference scheme; ——, regular viscous solution; A, channel profile; B, boundary-layer profile; C, Blasius profile.

Application of (19) and (20), Lin's formulae, provides an R^*_{cr} versus X^* curve similar to those from the asymptotic solutions. It is close to the curve from the composite solution and, in addition, exhibits the same pattern.

Finally, a plot is constructed to show the critical Reynolds number as a function of the physical axial location $X(=\bar{x}/LR^*)$ for both the channel profile and the boundary layer profile (figure 7). Only the results from the regular viscous solution and from the finite-difference scheme are included.

It is apparent from the figure that the analytical and numerical methods of solution yield consistent results for each flow model. The numerical method

provides somewhat higher critical Reynolds numbers than the analytical solution method. It is noteworthy that both flow models, i.e. channel and boundary layer, predict almost identical critical Reynolds numbers at small values of X, i.e. near the entrance of the channel. On the other hand, an increasing deviation is in evidence as X increases. The inset in the figure illustrates, in enlarged scale, the critical Reynolds numbers for small values of X.

For the purpose of examining how the stability boundary for Blasius flow over a flat plate compares with that for the channel flow, two curves from the former are also included in figure 7. These curves were calculated from the expression

$$R^* = (R_{x,B}/XU_{\max})^{\frac{1}{2}}, \tag{21}$$

where $R_{x,B}(=\overline{x}\overline{u}_{\max}/\nu)$, the Reynolds number for Blasius flow, is related to $R_{\delta^*} = (\overline{\delta}^*\overline{u}_{\max}/\nu)$, the Reynolds number based on the displacement thickness $\overline{\delta}^*$, by (see Schlichting 1960)

$$R_{\delta^*} = 1{\cdot}72(R_{x\,B})^{\frac{1}{2}}. \tag{22}$$

The critical Reynolds numbers $R_{\delta^*,\mathrm{cr}}$ for the Blasius flow have been found to be 420 for the regular viscous solution (Lin 1945) and 530 for the finite-difference scheme (Kurtz & Crandall 1962).

It can be seen from the figure that the R^*_{cr} values for the Blasius profile are very much smaller than those for the channel profile. However, it is evident that as X approaches zero, all of the profiles give R^*_{cr} values that approach infinity.

9. Concluding remarks

From the results of this investigation, the following major conclusions are drawn.

The critical Reynolds number R^*_{cr} or R_{cr} decreases monotonically with increasing distance from the channel entrance, approaching the fully developed value as a limit. This finding is physically significant because it suggests that flow instability in a carefully controlled experiment will occur in the fully developed region rather than in the entrance region.

The boundary-layer model, in general, predicts higher critical Reynolds numbers than the channel model.

Both the channel and the boundary-layer models predict essentially identical critical Reynolds numbers in the region very near the entrance of the channel.

The boundary-layer model is not a valid approach for investigating stability in the downstream portion of the hydrodynamic entrance region.

Among the various asymptotic solutions, the regular viscous solution yielded the most accurate results. This is believed due to the close proximity of the turning point to the wall for the basic flow under consideration.

The approximate formulae of Lin fail to give accurate critical Reynolds numbers in the development region, except for velocity profiles very close to the fully developed.

The authors wish to thank Dr Daniel D. Joseph of the Department of Aeronautics and Engineering Mechanics, University of Minnesota, for many helpful

discussions throughout the course of investigation. The partial financial support to one of us (T.S.C.) under NASA grant (NGR-24-005-065-) is also gratefully acknowledged.

REFERENCES

CHEN, T. S. 1966 Hydrodynamic stability of developing flow in a parallel-plate channel. Ph.D. Thesis, Department of Mechanical Engineering, University of Minnesota.

CHEN, T. S., JOSEPH, D. D. & SPARROW, E. M. 1966 *Phys. Fluids*, **9**, 2519.

FU, T. S. 1967 Viscous instability of asymmetric parallel flows in channels. Ph.D. Thesis Department of Aeronautics and Engineering Mechanics, University of Minnesota.

GRÖHNE, D. 1954 *Z. Angew. Math. Mech.* **34**, 344.

HAHNEMAN, E., FREEMAN, J. C. & FINSTON, M. 1948 *J. Aero. Sci.* **15**, 493.

HEISENBERG, W. 1924 *Ann. Phys.* **74**, 577.

HOLSTEIN, H. 1950 *Z. Angew. Math. Mech.* **30**, 25.

KURTZ, E. F. & CRANDALL, S. H. 1962 *J. Math. Phys.* **41**, 264.

LIN, C. C. 1945 *Quart. Appl. Math.* **3**, 117, 213, 277.

LIN, C. C. 1955 *The Theory of Hydrodynamic Stability*. Cambridge University Press.

LOCK, R. C. 1954 *Proc. Camb. Phil. Soc.* **50**, 105.

MILES, J. W. 1960 *J. Fluid Mech.* **8**, 593.

NACHTSHEIM, P. R. 1964 *NASA TN* D-2414.

REID, W. H. 1965 The stability of parallel flows. In *Basic Development in Fluid Mechanics*. Ed. by M. Holt. New York: Academic Press.

SCHLICHTING, H. 1934 *Z. Angew. Math. Mech.* **14**, 368.

SCHLICHTING, H. 1960 *Boundary Layer Theory*. New York: McGraw-Hill.

SHEN, S. F. 1964 Stability of laminar flows. In *Theory of Laminar Flows*. Ed. by F. K. Moore, Princeton University Press.

SPARROW, E. M., LIN, S. H. & LUNDGREN, T. S. 1964 *Phys. Fluids*, **7**, 338.

STUART, J. T. 1963 Hydrodynamic stability. In *Laminar Boundary Layers*. Ed. by L. Rosenhead. Oxford University Press.

THOMAS, L. H. 1953 *Phys. Rev.* **91**, 780.

TIETJENS, O. 1925 *Z. Angew. Math. Mech.* **5**, 200.

TOLLMIEN, W. 1929 *Nachr. Ges. Wiss. Göttingen, Math.-Phys. Klasse*, p. 21.

TOLLMIEN, W. 1947 *Z. Angew. Math. Mech.* **25–27**, 33, 70.

TSOU, F. K. 1965 Velocity field, hydrodynamic stability, and heat transfer for boundary-layer flow along a continuous moving surface. Ph.D. Thesis, Department of Mechanical Engineering, University of Minnesota.